Reversible Dioxygen Binding to Hemerythrin. 2. Mechanism of the Proton-Coupled Two-Electron Transfer to O_2 at a Single Iron Center

Thomas C. Brunold and Edward I. Solomon*

Contribution from the Department of Chemistry, Stanford University, Stanford, California 94305

Received February 2, 1999

Abstract: In the reaction of the binuclear non-heme iron protein hemerythrin (Hr) with dioxygen, one electron from each Fe(II) center and the proton from the bridging hydroxide of the diferrous site (deoxyHr) are transferred to O_2 binding to a single iron center (Fe2), yielding the oxo-bridged diferric site possessing a terminal hydroperoxide (oxyHr). Using the experimentally calibrated bonding descriptions of oxyHr and deoxyHr developed in the accompanying paper [Brunold, T. C.; Solomon, E. I. *J. Am. Chem. Soc.* **1999**, *121*, 8277], the process of O_2 release from Hr is explored through density functional calculations that interpolate between these well-defined reference electronic structures. The relevant steps are (i) elongation of the Fe2−hydroperoxide bond driving the first one-electron transfer (ET) from the peroxide to the coordinated iron (Fe2), followed by (ii) tunneling of the hydroperoxide proton to the μ-oxo bridge coupled with the second ET, from the O_2 species to the noncoordinated iron (Fe1). Significantly, while (ii) is a proton-coupled ET it is not an H atom transfer as the electron transfers through the same Fe−O−Fe mixed σ/π superexchange pathway that produces the dominant contribution to the strong antiferromagnetic coupling in oxyHr and bent oxo-bridged diferric complexes in general.

1. Introduction

Hemerythrins (Hr) constitute one of the three classes of metalloproteins capable of reversible binding of dioxygen.[1] They differ fundamentally from the hemoglobins[2] and hemocyanins[3] in possessing an active site with two exchange-coupled non-heme iron centers.[1,4] Oxygenation of the hydroxo-bridged diferrous deoxyHr site[4−6] involves a one-electron transfer (ET) from each Fe(II) ion coupled with a proton transfer (PT) from the bridging hydroxide to O_2 binding at a single metal center, yielding the oxo-bridged diferric oxyHr site possessing a terminal hydroperoxide[4,7,8] that is hydrogen-bonded[9] to the oxo bridge (Chart 1). Despite the large body of existing experimental data for deoxyHr, oxyHr, and their interconversion,[1,10] the complexity of the O_2 binding process has so far limited insight into the reaction mechanism.[11] In particular, the order in which the two electrons and the proton are transferred to O_2 has yet to be established,[1] and the correlation of spin states for this reaction of triplet O_2 with the weakly antiferromagnetically coupled deoxyHr site,[12] $J = -14$ cm^{-1} ($H = -2J\mathbf{S}_1\cdot\mathbf{S}_2$), yielding the strongly antiferromagnetically coupled oxyHr site,[13] $J = -77$ cm^{-1}, remains to be explored.

Chart 1. Reversible O_2 Binding to Hr

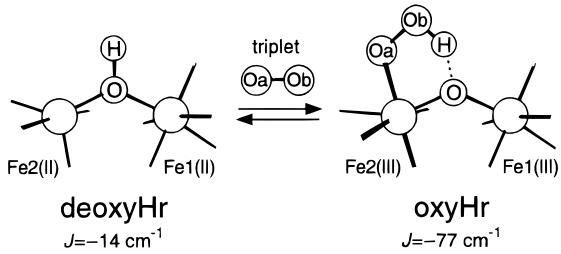

Recent advances in computational chemistry have permitted detailed electronic structure studies on metalloprotein active sites, such as methane monooxygenase,[14] nitrogenase,[15] hydrogenase,[16] tyrosinase,[17] and the oxygen-evolving complex,[18] which have significantly contributed to the current understanding of the reactivity of these sites. In this paper, the mechanism of reversible dioxygen binding to Hr is explored by utilizing density functional calculations that interpolate between the experimentally calibrated bonding descriptions of oxyHr and deoxyHr generated in the accompanying paper.[12] Analysis of the reaction coordinate corresponding to hydroperoxide dissociation from oxyHr coupled to proton transfer from the O_2 species to the

(1) Stenkamp, R. E. *Chem. Rev.* **1994**, *94*, 715.
(2) Niederhoffer, E. C.; Timmons, J. H.; Martell, A. E. *Chem. Rev.* **1984**, *84*, 137.
(3) Solomon, E. I.; Baldwin, M. J.; Lowery, M. D. *Chem. Rev.* **1992**, *92*, 521.
(4) Holmes, M. A.; Le Trong, I.; Turley, S.; Sieker, L. C.; Stenkamp, R. E. *J. Mol. Biol.* **1991**, *218*, 583.
(5) (a) Reem, R. C.; Solomon, E. I. *J. Am. Chem. Soc.* **1984**, *106*, 8323. (b) Reem, R. C.; Solomon, E. I. *J. Am. Chem. Soc.* **1987**, *109*, 1216.
(6) Maroney, M. J.; Kurtz, D. M., Jr.; Nocek, J. M.; Pearce, L. L.; Que, L., Jr. *J. Am. Chem. Soc.* **1986**, *108*, 6871.
(7) Gay, R. R.; Solomon, E. I. *J. Am. Chem. Soc.* **1978**, *100*, 1972.
(8) Reem, R. C.; McCormick, J. M.; Richardson, D. E.; Devlin, F. J.; Stephens, P. J.; Musselman, R. L.; Solomon, E. I. *J. Am. Chem. Soc.* **1989**, *111*, 4688.
(9) Shiemke, A. K.; Loehr, T. M.; Sanders-Loehr, J. *J. Am. Chem. Soc.* **1984**, *106*, 4951.
(10) (a) Wilkins, P. C.; Wilkins, R. G. *Coord. Chem. Rev.* **1987**, *79*, 195. (b) Klotz, I. M.; Kurtz, D. M., Jr. *Acc. Chem. Res.* **1984**, *17*, 16.
(11) Bosnich, B. *Inorg. Chem.* **1999**, *38*, in press.
(12) Brunold, T. C.; Solomon, E. I. *J. Am. Chem. Soc.* **1999**, *121*, 8277.
(13) Dawson, J. W.; Gray, H. B.; Hoenig, H. E.; Rossman, G. R.; Schredder, J. M.; Wang, R. H. *Biochemistry* **1972**, *11*, 461.
(14) (a) Siegbahn, P. E. M.; Crabtree, R. H. *J. Am. Chem. Soc.* **1997**, *119*, 3103. (b) Siegbahn, P. E. M. *Inorg. Chem.* **1999**, *38*, in press.
(15) (a) Stavrev, K. K.; Zerner, M. C. *Theor. Chem. Acc.* **1997**, *96*, 141. (b) Siegbahn, P. E. M.; Westerberg, J.; Svensson, M.; Crabtree, R. H. *J. Phys. Chem. B* **1998**, *102*, 1615.
(16) Pavlov, M.; Siegbahn, P. E. M.; Blomberg, M. R. A.; Crabtree, R. H. *J. Am. Chem. Soc.* **1998**, *120*, 548.
(17) (a) Ross, P. K.; Solomon, E. I. *J. Am. Chem. Soc.* **1991**, *113*, 3246. (b) Lind, T.; Siegbahn, P. E. M.; Crabtree, R. H. *J. Phys. Chem. B* **1999**, *103*, 1193.
(18) (a) Schmitt, E. A.; Noodleman, L.; Baerends, E. J.; Hendrickson, D. N. *J. Am. Chem. Soc.* **1992**, *114*, 6109. (b) Blomberg, M. R. A.; Siegbahn, P. E. M.; Styring, S.; Babcock, G. T.; Åkermark, B.; Korall, P. *J. Am. Chem. Soc.* **1997**, *119*, 8285. (c) McGrady, J. E.; Stranger, R. *Inorg. Chem.* **1999**, *38*, 550. (d) Siegbahn, P. E. M.; Crabtree, R. H. *J. Am. Chem. Soc.* **1999**, *121*, 117.

10.1021/ja992234s CCC: $18.00
Published on Web 08/31/1999

bridging oxide provides significant new insight into the nature of the ET mechanisms, the sequence in which the ET and PT events occur, the correlation of spin states, and the role of antiferromagnetic exchange coupling through the bridging oxide in ET.

2. Experimental Section

Density functional calculations were performed on IBM 3BT-RS/6000 work stations using the Amsterdam density functional (ADF) program version 2.0.1 developed by Baerends and co-workers.[19] A triple-ζ Slater-type orbital basis set (ADF basis set IV), extended with a single polarization function, was used to describe each atom. The frozen core approximation was employed for core orbitals through 1s (N, O) and 3p (Fe). All calculations were performed using the local density approximation of Vosko, Wilk, and Nusair[20] for the exchange and correlation energy and the nonlocal gradient corrections to exchange and correlation by Becke[21] and Perdew,[22] respectively. Geometry optimizations were carried out by utilizing the algorithm of Versluis and Ziegler[23] provided in the ADF package and were considered converged when the gradient and changes in coordinates between subsequent iterations fell below 0.01 hartree/Å and 0.01 Å, respectively.

The active site structures of deoxyHr and oxyHr were approximated by models in which formates replace the carboxylates and NH_3 ligands replace the histidines (see ref 12). While this type of modeling may have a substantial effect on the calculated energy profile,[24] evaluations on the basis of spectroscopic data have shown that the calculated electronic structure descriptions of the deoxyHr and oxyHr models employed are reasonable (see the accompanying paper[12]). Therefore, the use of these approximate models, which is necessary for a quantum mechanical treatment of this system, appears to be sufficient to permit identification of the key steps in the reaction of Hr with O_2. Complete coordinates of all the models presented in the text are included in the Supporting Information.

3. Results and Analysis

In this section, the reaction coordinate for the conversion of oxyHr into deoxyHr is analyzed. First, the effects upon the experimentally calibrated electronic structure description of oxyHr[12] are explored of transferring the proton from the hydroperoxide to the bridging oxide. On the basis of these results the hydroperoxide dissociation reaction starting from oxyHr is evaluated, and important aspects, including the correlation of spin states and the role of antiferromagnetic exchange coupling, are addressed in the subsequent sections.

Effects of Hydroperoxide → μ-Oxo Proton Transfer in OxyHr. From electronic structure studies on the oxyHr site,[12] protonation greatly reduces the σ-donor interaction of the peroxide with Fe2 (see Chart 1 for atom designations), suggesting that transfer of the proton from the O_2 species to the bridging oxide might play a key role in the process of dioxygen release from oxyHr. Therefore, broken symmetry (BS, $M_S = 0$) electronic structure calculations were performed on the μ-OH,O_2 model in Figure 1 (right) that was derived from oxyHr (left) by transferring the hydroperoxide proton to the bridging oxide and reoptimizing the Oa, Ob, H, and O coordinates. To prevent reconvergence to the oxyHr structure because of the large difference in pK_a of a hydroxo bridge in ferric dimers[25]

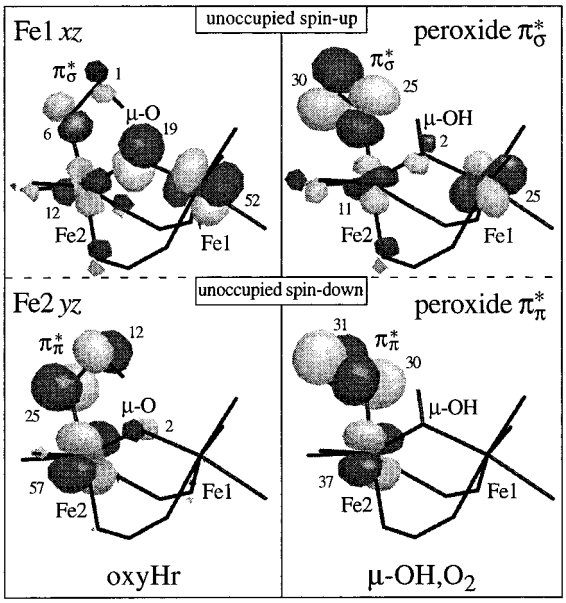

Figure 1. Surface plots of the unoccupied Fe1 *xz*/peroxide π^*_σ-based spin-up and Fe2 *yz*/peroxide π^*_π-based spin-down MOs obtained from BS calculations on oxyHr and μ-OH,O_2. The O p and Fe d orbital contributions are indicated.

(~2.0−3.5) and hydrogen peroxide[26] (11.6), it was necessary to eliminate the Ob···H interactions by rotating the peroxide around the Fe2−Oa bond by 180°. An energy level for μ-OH,O_2 is shown in Figure S1 (Supporting Information).

Conversion of oxyHr into μ-OH,O_2 results in a significant electron redistribution, most dramatically in a large increase in the peroxide → Fe charge donation at the expense of the μ-O(H) donor strength: the spin-up Fe1 *xz*-based and spin-down Fe2 *yz*-based unoccupied molecular orbitals (MOs) in oxyHr gain predominant peroxide π^* character in μ-OH,O_2 (Figure 1), indicating that their occupied bonding counterparts (not shown[27]) now have primarily iron d character. Thus, the hydroperoxide → μ-oxo PT is formally coupled with a peroxide → Fe two-electron transfer occurring at a single iron center, a spin-up electron from the peroxide π^*_σ orbital (located in the O_2H plane and σ-bonding to Fe2) to Fe1 *xz* and a spin-down electron from the π^*_π orbital (oriented perpendicular to the O_2H plane and π-bonding to Fe2) to Fe2 *yz*. Initiation of dioxygen release from oxyHr through PT from the hydroperoxide to the bridging oxide is rather unlikely, however: (i) the pK_a values are such that the potential energy surface (PES) of the proton has no local minimum for Ob···H−μ-O, and therefore, the rate for proton transfer will be negligible,[28] and (ii) a large H/D kinetic isotope effect (KIE) would be expected in that case, contrasting the small observed KIE[29] of ~1.0 (1.2) for dioxygen binding (release).[30] Alternatively, dioxygen release could be initiated by dissociation of the hydroperoxide from Fe2, as considered in the next section.

Hydroperoxide Dissociation from OxyHr. The reaction coordinate of hydroperoxide dissociation from oxyHr was studied by varying, in discrete steps, the Fe2−Oa(hydroperox-

(19) (a) Baerends, E. J.; Ellis, D. E.; Ros, P. *Chem. Phys.* **1973**, *2*, 42. (b) te Velde, G.; Baerends, E. J. *Int. J. Comput. Phys.* **1992**, *99*, 84.

(20) Vosko, S. H.; Wilk, L.; Nusair, M. *Can. J. Phys.* **1980**, *58*, 1200.

(21) Becke, A. D. *J. Chem. Phys.* **1986**, *84*, 4524.

(22) Perdew, J. P. *Phys. Rev. B* **1986**, *33*, 8822.

(23) Versluis, L.; Ziegler, T. *J. Chem. Phys.* **1988**, *88*, 322.

(24) A quantitative analysis of the energy profile for the interconversion of oxyHr and deoxyHr (which is beyond the scope of this study) would require full geometry optimizations and corrections for zero-point vibrational energies for all the models used to define the reaction coordinate. Further, highest accuracy for energy calculations might be anticipated from hybrid density functional calculations at the B3LYP level rather than from the gradient-corrected method employed in this study.

(25) (a) Armstrong, W. H.; Lippard, S. *J. Am. Chem. Soc.* **1984**, *106*, 4632. (b) Turowski, P. N.; Armstrong, W. H.; Liu, S.; Brown, S. N.; Lippard, S. *Inorg. Chem.* **1994**, *33*, 636.

(26) Holm, R. H.; Kennepohl, P.; Solomon, E. I. *Chem. Rev.* **1996**, *96*, 2239.

(27) Exchange stabilization of the Fe d-based occupied MOs results in significant mixing with ligand-based orbitals, which complicates a direct analysis of the occupied orbitals. The metal−ligand bonding interactions are therefore inferred from the Fe d-based unoccupied MOs that are metal−ligand antibonding in nature.

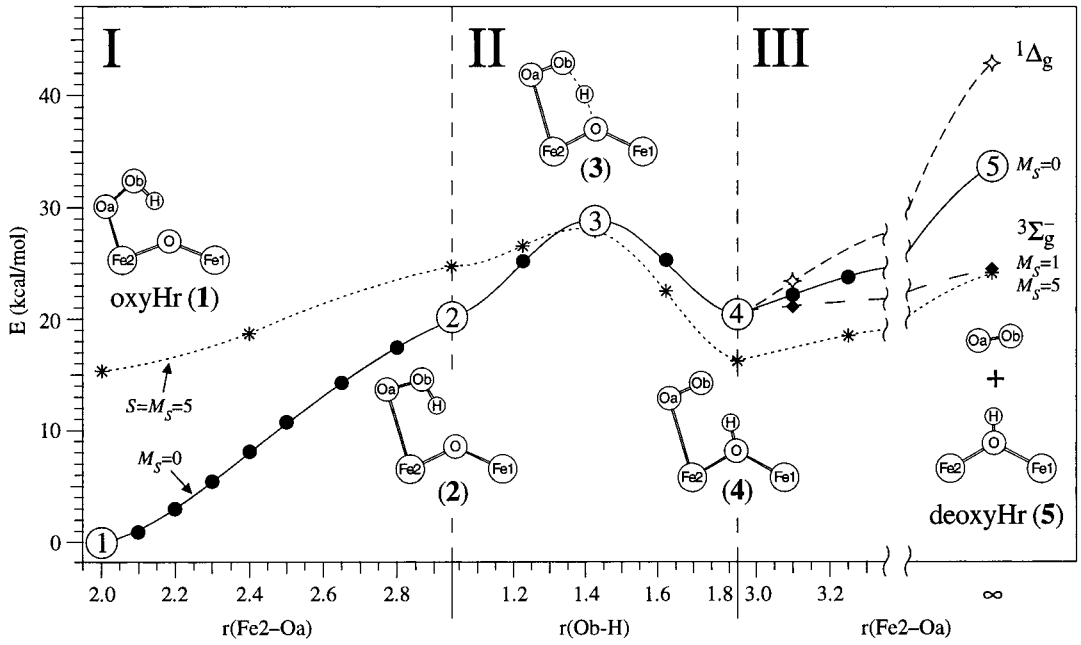

Figure 2. Calculated potential energy surfaces for the interconversion of oxyHr (**1**, left) and deoxyHr (**5**, right) as a function of the Fe2−Oa distance (regions I and III) and the Ob−H distance (region II, with r(Fe2−Oa) = 2.95 Å). Each curve corresponds to a different spin state: (●)/solid line for $M_S = 0$; (*)/dotted line for $S = 5$; (◆)/long dashes for $S = 1$ ($^3\Sigma_g^-$) O_2 and $M_S = 0$ deoxyHr; (◇)/short dashes for $S = 0$ ($^1\Delta_g$) O_2 and $M_S = 0$ deoxyHr.

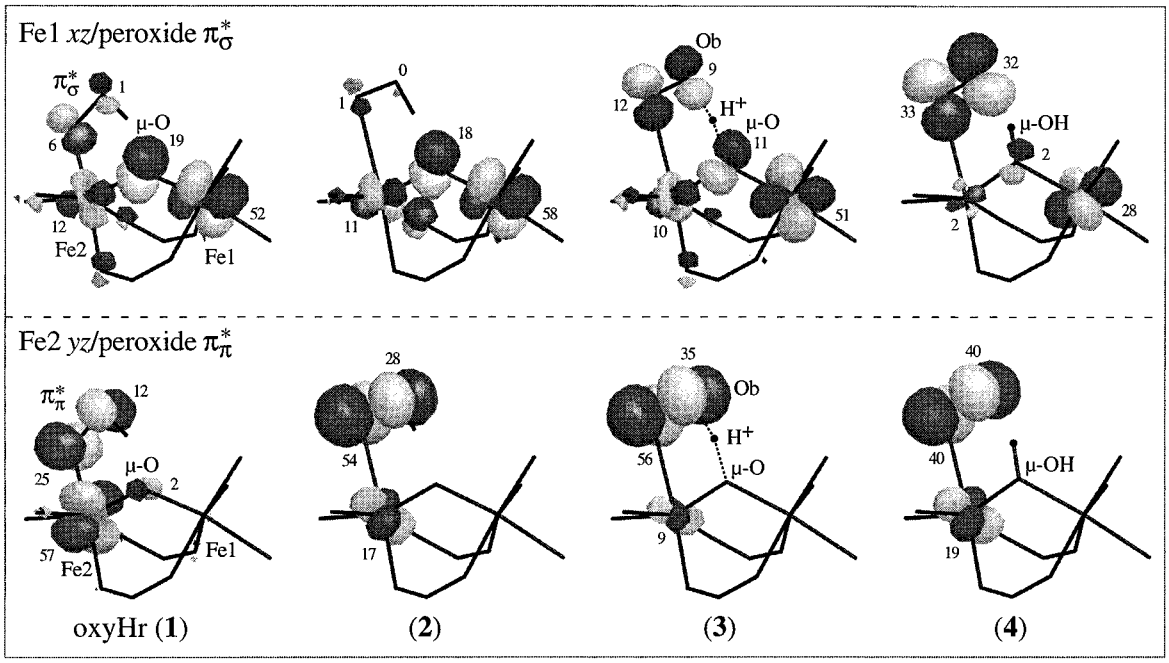

Figure 3. Surface plots of the unoccupied Fe1 *xz*/peroxide π^*_σ-based spin-up and Fe2 *yz*/peroxide π^*_π-based spin-down MOs obtained from BS calculations on structures **1** (oxyHr) through **4** in Figure 2. The O p and Fe d orbital contributions are indicated.

ide) bond length and reoptimizing the coordinates of the Ob−H···μ-O atoms. The corresponding PES is shown in Figure 2, region I (solid line), and an overlay plot of the optimized HO_2−Fe−O−Fe core structures is presented in Figure S2 (Supporting Information). While an increase in the Fe2−Oa distance from r(Fe2−Oa) = 2.00 Å in oxyHr (**1** in Figure 2) to 2.95 Å (**2**) results in a large increase in the total energy, changes in the Ob−H···μ-O positions are minor (Figure S2).

From the conversion of oxyHr into μ-OH,O_2 (Figure 1, *vide supra*), the key orbitals involved in the process of O_2 release from oxyHr are the spin-up Fe1 *xz*/peroxide π^*_σ-based and spin-down Fe2 *yz*/peroxide π^*_π-based orbitals. Corresponding surface plots for the unoccupied MOs of oxyHr (**1**) and structure **2** are shown in Figure 3 (left). The unoccupied Fe2 *yz*-derived level of oxyHr becomes predominantly peroxide π^*_π in character in complex **2**, indicating that substantial spin-down electron density has shifted from peroxide to Fe2 in the bonding orbital, whereas the Fe1 *xz*/peroxide π^*_σ-based MO is only slightly affected. Thus, in contrast to the PT discussed above, hydro-

(28) Cukier, R. I.; Zhu, J. *J. Phys. Chem. B* **1997**, *101*, 7180.
(29) Armstrong, G. D.; Sykes, A. D. *Inorg. Chem.* **1986**, *25*, 3135.
(30) This model is consistent with the observation that no intermediates are detected in the deoxygenation process of oxyHr.[29]

Chart 2. Variation of the Proton PES as a Function of *r*(Fe2−Oa) (Figure 2, region I)

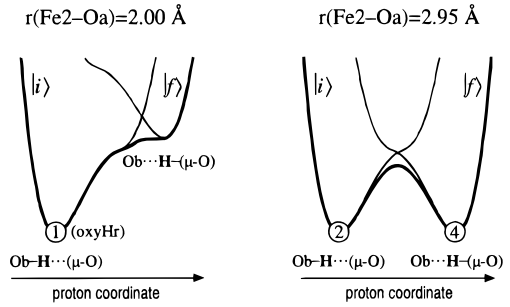

peroxide dissociation from oxyHr drives a single ET, a spin-down electron from peroxide π^*_π to Fe2 *yz*.

Proton-Coupled Electron Transfer. Transfer of electron density from the hydroperoxide to Fe2 with increasing Fe2−Oa distance (Figure 3) formally produces a hydrosuperoxide at the μ-O Fe1(III)/Fe2(II) site of complex **2**. Given the lower pK_a of hydrosuperoxide[26] (4.9) than that of the bridging hydroxide at the Fe(II)/Fe(III) site of halfmetHr[31] (>9), a minimum is expected to develop in the proton PES for peroxide Ob···H−μ-O as the Fe2−Oa distance increases. This was probed through calculations similar to the ones discussed above, but with the proton transferred from Ob to the bridging oxide. The relevant part of the corresponding PES is shown in Figure 2, region III (solid line).

From Figure 2, the PESs for peroxide Ob−H···μ-O (region I) and Ob···H−μ-O (region III) cross at *r*(Fe2−Oa) ≈ 2.95 Å. Thus, in this configuration the oxo-bridged structure **2** possessing a protonated O_2 species and the hydroxo-bridged structure **4** having a deprotonated O_2 moiety (cf. Figure 2) are isoenergetic, the hydroxo-bridged site being more stable at larger Fe2−Oa distances. The dependence of the proton PES on *r*(Fe2−Oa) is schematically illustrated in Chart 2. For oxyHr (**1**) the pK_a values of the hydroperoxide and the bridging oxide are such that the proton PES only has a peroxide Ob−H···μ-O localized state. With increasing *r*(Fe2−Oa), i.e., increasing hydroperoxide → Fe2 charge donation, a μ-O localized state develops and the proton PES eventually becomes isoenergetic for structures **2** (Ob−H···μ-O) and **4** (Ob···H−μ-O). In this configuration (Chart 2, right), the proton can tunnel through the barrier between the Ob and μ-O localized states at a rate depending on the strength of the coupling between the initial and final states.[28]

To quantitate the tunneling rate for the PT process **2** → **4**, the proton PES was defined through BS calculations on structures that interpolate between complexes **2** and **4**[32] (i.e., for *r*(Fe2−Oa) = 2.95 Å). The PES obtained (Figure 2, solid line in region II) was then modeled by the following quartic potential:[28,33,34]

$$V(X) = \frac{\hbar\omega}{2}\left[-\frac{1}{2}X^2 + cX^4\right] \qquad (1)$$

where $X = (\mu\hbar\omega)^{1/2}(r(\mathrm{Ob{-}H}) - r_0)$, μ is the reduced mass (approximated by the proton mass), *c* is a fit parameter, and r_0=1.43 Å is the Ob−H distance in the transition state with the proton halfway between the O_2 species and the bridging oxide (Figure 2, structure **3** in region II). The proton surface calculated with the fitted Ob−H stretching frequency of $\hbar\omega = 2300$ cm^{-1} (consistent with a strong hydrogen bond interaction[34]) is plotted in Figure 4 along with the energies and wave functions obtained by numerically solving the vibrational Hamiltonian. The double-well potential in Figure 4 is sufficiently deep and wide that the PT problem can be reduced to a two-level system (υ = 0, 1), because the higher vibrational states are too high in energy to significantly contribute to the transfer process. The splitting between the υ = 0 and 1 levels, $\Delta E_\pm = 11$ cm^{-1}, is related to the tunneling rate constant by[35] $k_{PT} = \Delta E_\pm/h$, yielding $k_{PT} = 6.9 \times 10^{11}$ s^{-1}.[36] The PT step is therefore not expected to make a significant contribution to the rate constants for O_2 binding and release (7.4×10^6 M^{-1} s^{-1} and 51 s^{-1}, respectively[37]), consistent with the small observed KIE (1.0 and 1.2, respectively[29]).

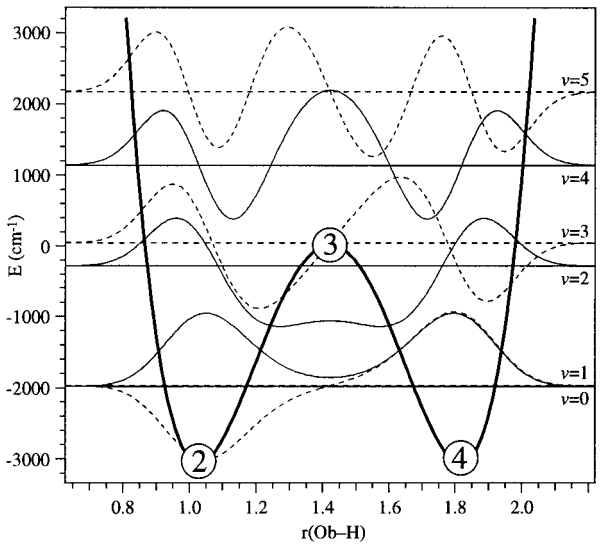

Figure 4. Proton PES as a function of the Ob−H distance (with r(Fe2−Oa) = 2.95 Å) obtained from a fit of eq 1 to region II in Figure 2 (for M_S = 0). Energies and wave functions of the protonic states from numerical solutions to the vibrational Hamiltonian are shown by solid lines (even states) and broken lines (odd states).

Boundary surface plots of the relevant unoccupied orbitals for complexes **3**, the transition state, and **4**, the final (hydroxo-bridged) state, in the PT reaction **2** → **4** are included in Figure 3. While the peroxide (which is formally oxidized to the superoxide level in **2**) π^*_π-based orbital is only slightly affected by the PT, the π^*_σ character in the unoccupied Fe1 *xz*-based MO increases along the reaction coordinate from complex **2** to **3** and further to **4** where the peroxide now makes the dominant contribution. Thus, the PT event **2** → **4** is formally coupled with a spin-up peroxide π^*_σ → Fe1 *xz* ET. Proton-coupled ET reactions have recently been under intense study, and a model has been developed by Cukier[33,34] to distinguish between a consecutive mechanism, ET from the inital $|i\rangle$ to the final $|f\rangle$ electronic states for a fixed proton position (e.g., Ob−H···μ-O in Chart 2) followed by PT (ET/PT), and a concerted mechanism where the electron and proton transfer simultaneously (ETPT). In the present case, an ET/PT mechanism would require that

(31) McCormick, J. M.; Reem, R. C.; Solomon, E. I. *J. Am. Chem. Soc.* **1991**, *113*, 9066.
(32) A transition-state calculation could result in a lower barrier height of the double-well potential. Thus, the calculated proton tunneling rate constant ($k_{PT} = 6.9 \times 10^{11}$ s^{-1}) provides a lower limit.
(33) Cukier, R. I. *J. Phys. Chem.* **1995**, *99*, 16101.
(34) Cukier, R. I. *J. Phys. Chem.* **1996**, *100*, 15428.
(35) Cohen-Tannoudji, C.; Diu, B.; Laloë, F. *Quantum Mechanics*; John Wiley & Sons: New York, 1977; Vol. 1, pp 455−469.
(36) As pointed out by a reviewer, the rate constant for the PT obtained using classical transition-state theory is about 3 orders of magnitude smaller than the calculated tunneling rate constant ($k_{PT} = 6.9 \times 10^{11}$ s^{-1}), indicating that the strong hydrogen bond in oxyHr facilitates rapid PT.
(37) de Waal, D. J. A.; Wilkins, R. G. *J. Biol. Chem.* **1976**, *251*, 2339.

the $|f\rangle$ PES supports an Ob−H···μ-O localized state. This was probed by modeling the $|f\rangle$ PES from the energies of the peroxide $\pi^*_\sigma \rightarrow$ Fe1 *xz* CT excited state for complex **2** and structures that interpolate between **2** and **3**. It was found that the energy of the CT excitation is large, about 10000 cm^{-1} for **2**, and that the $|f\rangle$ PES has no minimum for Ob−H···μ-O. Thus, an ET/PT mechanism is not supported by the calculations,[33,34] leaving ETPT as the likely reaction channel. The strong coupling between the initial and final states in this ETPT process, reflected in the large proton tunneling rate constant, indicates that the ET occurs adiabatically,[38] i.e., gradually with distortion along the proton coordinate.

The pathway for the proton-coupled peroxide $\pi^*_\sigma \rightarrow$ Fe1 *xz* ET process **2** → **4** can be inferred from the MO boundary surface plots in Figure 3. Strikingly, in complex **3** (the transition state) the unoccupied Fe1 *xz*/peroxide π^*_σ MO has considerable μ-oxo and Fe2 orbital character, and the Fe2−O−Fe1 orbital configuration bears striking similarities to the mixed σ/π superexchange pathway that produces the dominant contribution to the strong antiferromagnetic coupling in oxyHr[12] (Figure 3, structure **1** (top)). These results suggest that *the proton-coupled ET from peroxide to Fe1 involves the Fe2−O−Fe1 mixed σ/π superexchange pathway rather than a hydrogen atom transfer in which case the electron would transfer together with the proton*. This model is consistent with the insignificant change in proton charge in the ETPT process (Figure S3, Supporting Information), as a hydrogen atom transfer would result in a substantial decrease in proton charge.

In summary, the two key steps for the transformation of oxyHr into deoxyHr are (i) hydroperoxide dissociation driving a spin-down ET from the peroxide π^*_π orbital to Fe2 followed by (ii) proton tunneling from Ob−H···μ-O to Ob···H−μ-O coupled with a spin-up ET from the peroxide π^*_σ orbital to Fe1 through the Fe2−O−Fe1 mixed σ/π superexchange pathway (Figure 3, structure **3** (top)). This model is based on the assumption that the ETPT event occurs at a fixed Fe2−Oa distance, which obscures the fact that the two-electron one-proton-transfer reaction of O_2 release from oxyHr should actually have some concerted character. In any case the two ETs from peroxide to Fe2 and Fe1 are coupled to the hydroperoxide dissociation and the PT, respectively.

Spin Conservation and the Role of Exchange Coupling. In the previous sections the reaction coordinate of hydroperoxide dissociation from oxyHr (**1** → **4** in Figures 2 and 3) was analyzed for the $M_S = 0$ BS state that corresponds to a mixture of $M_S = 0$ components of the pure spin states S whose contributions $A(S)$ are given by[39]

$$A(S) = \frac{(2S+1)(n!)^2}{(n-S)!(n+S+1)!} \qquad (2)$$

where n is the number of unpaired electrons on each monomer half. $A(S)$ values for deoxyHr ($n = 4$) and oxyHr ($n = 5$) are listed in Table 1, along with the corresponding Boltzmann populations at 300 K (obtained with the experimental J values of −14 and −77 cm^{-1}, respectively[12,13]). From Table 1, the BS state accounts reasonably well for the fact that at 300 K several spin states of the oxyHr and deoxyHr sites participate in the reaction. With respect to O_2, however, the $M_S = 0$ wave function $|\cdots\pi^{*-}_\sigma \pi^{*+}_\pi|$ correlates with a 1:1 mixture of the $^3\Sigma^-_g$ ground state and the $^1\Delta_g$ excited state at ∼7880 cm^{-1} (Figure 2, solid line in region III).[40] Thus, conversion of oxyHr into deoxyHr (complex **5**) on the BS surface formally produces a mixture of singlet and triplet O_2, even though one electron is removed from each of the two peroxide π^* orbitals.

Table 1. Contributions $A(S)$ from the Pure Spin States S to the BS ($M_S = 0$) States of DeoxyHr and OxyHr (Obtained with Eq 2) and Corresponding Boltzmann Populations $\rho(S)$ at 300 K Obtained with $J = -14$ and -77 cm^{-1}, Respectively[12,13] (%)

	deoxyHr		oxyHr	
S	$A(S)$	$\rho(S)$	$A(S)$	$\rho(S)$
0	20	8	17	33
1	40	21	36	47
2	29	27	30	18
3	10	25	14	3
4	1	19	4	0
5			0	0

To explore in more detail the correlation of spin states for the interconversion of oxyHr and deoxyHr, calculations were performed on $M_S \neq 0$ states of relevant structures along the reaction coordinate. As shown in Figure 2 (asterisks in region I) in oxyHr (**1**) the high spin (HS, $S = 5$) state is significantly destabilized from the BS state (see ref 12 for a detailed discussion), consistent with the experimentally observed strong antiferromagnetic coupling[13] ($J = -77$ cm^{-1}). In the framework of the valence bond configuration interaction model[41] that provided significant insight into the origin of exchange coupling in oxo-bridged ferric dimers,[42] the ground-state antiferromagnetism results from second-order configuration interaction with metal-to-metal CT (MMCT) and double CT (DCT) excited states. Due to lack of $S = 5$ MMCT and DCT excited states, the HS ground state is not stabilized in energy, and the contribution from exchange coupling to the net stabilization of the singlet ground state in oxyHr can be estimated[43] from the energy difference between the $S = 0$ and HS ($S = 5$) spin states. With the experimental exchange coupling constant[13] of $J = -77$ cm^{-1} a value of 2310 cm^{-1} or 6.6 kcal/mol is obtained, indicating that the strong antiferromagnetic exchange coupling in oxyHr produces a substantial enthalpic contribution to the driving force for O_2 binding to Hr.

With progess along the reaction coordinate from oxyHr (**1**) to **2** (Figure 2, region I), the splitting between the HS and BS states, which is proportional to J,[39] gradually decreases due to a (partial) reduction of Fe2 that localizes this center and greatly reduces Fe1 → Fe2 electron delocalization. In the subsequent PT tunneling process **2** → **4**, a crossover of the HS and BS surfaces occurs (Figure 2, dotted and solid lines, respectively, in region II) such that in the hydroxo-bridged structure **4** the ferromagnetic HS state is shifted below the antiferromagnetic BS state. In complex **4** the O_2 species is formally oxidized to the dioxygen level (cf. the previous section); thus, given the large stabilization of triplet vs singlet O_2, it is not surprising that in **4** the HS state, correlating with the ferromagnetic $S = 4$ state of deoxyHr (**5**) and triplet dioxygen (Figure 2, dotted line in region III), is lower in energy than the BS state, correlating with the $M_S = 0$ state of deoxyHr and a 1:1 mixture of singlet and triplet O_2 (Figure 2, solid line in region III). It might have been anticipated that the lowest energy for structure **4** would be obtained for triplet O_2 interacting with the antiferromagnetic

(38) (a) Newton, M. D. *Chem. Rev.* **1991**, *91*, 767. (b) Barbara, P. F.; Meyer, T. J.; Ratner, M. A. *J. Phys. Chem.* **1996**, *100*, 13148.
(39) Noodleman, L. *J. Chem. Phys.* **1981**, *74*, 5737.
(40) Klotz, R.; Marian, C. M.; Peyerimhoff, S. D.; Hess, B. A.; Buenker, R. J. *Chem. Phys.* **1984**, *89*, 223.
(41) Tuczek, F.; Solomon, E. I. *Inorg. Chem.* **1993**, *32*, 2850.
(42) Brown, C. A.; Remar, G. J.; Musselman, R. L.; Solomon, E. I. *Inorg. Chem.* **1995**, *34*, 688.
(43) Bertrand, P.; Gayda, J.-P. *Biochim. Biophys. Acta* **1982**, *680*, 331.

Chart 3. Spin-State Dependence of the Bonding Interaction between O_2 and DeoxyHr

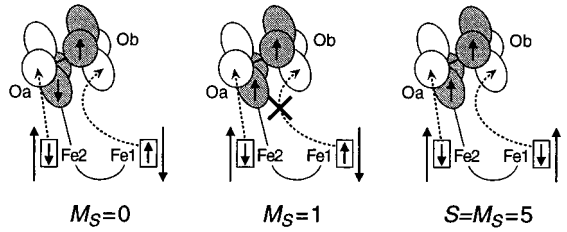

BS ($M_S = 0$) diferrous site, which can reasonably well be expressed by a single determinant, $|\cdots\pi_\sigma^{*+}\pi_\pi^{*+}|$. However, as indicated in Figure 2 (long dashes in region III), this $M_S = 1$ state lies slightly higher in energy than the BS ($M_S = 0$) state of **4**, indicating that one component of $^1\Delta_g$ dioxygen, i.e., $1/\sqrt{2}(|\pi_\sigma^{*+}\pi_\pi^{*-}| - |\pi_\sigma^{*-}\pi_\pi^{*+}|)$, has dropped below the $^3\Sigma_g^-$ state $|\pi_\sigma^{*+}\pi_\pi^{*+}|$. (The energy for the pure singlet ($S = 0$) dioxygen interacting with the $M_S = 0$ deoxyHr site can be estimated from the energies of the $M_S = 0$ and 1 states[39] (Figure 2, short dashes in region III)).

The origin of the energy variation with spin state based on differences in bonding interactions of singlet and triplet O_2 with deoxyHr is defined in Chart 3. In the BS ($M_S = 0$) state that, conceptionally, illustrates the interaction of singlet O_2 with the antiferromagnetically coupled deoxyHr site, the spin topology is such that both Fe(II) centers can shift charge onto dioxygen (indicated by the dotted arrows). Alternatively, in the $M_S = 1$ state only one iron (Fe2 in Chart 3) has proper spin alignment for charge donation to triplet O_2, leading to a destabilization of this state relative to the BS state as O_2 approaches the deoxyHr site. By contrast in the HS ($S = 5$) state, similar to the $M_S = 0$ state, both Fe(II) centers of the ferromagnetically coupled binuclear site can shift electron density onto triplet O_2. Because the antiferromagnetic exchange coupling in deoxyHr is weak[12] ($J = -14$ cm^{-1}), the more favorable electron correlation in triplet vs singlet O_2 outweighs the slightly unfavorable ferromagnetic alignment of Fe(II) spins, and the $S = 5$ state represents the ground state of complex **4** (Figure 2, asterisks in region III). Thus, with progress along the reaction coordinate from oxyHr (**1**) to **4** the spin state increases, which is viable in steps of $\Delta S = 1$ through a single-ion spin−orbit coupling (SOC) mechanism.[44] Though complex **4** has a HS ground state that correlates with triplet O_2 (Figure 2, dotted line in region III), the small energy separation of the BS state (correlating with a 1:1 mixture of singlet and triplet O_2) in this geometry suggests that initially some singlet dioxygen will also be released from oxyHr.

A schematic energy level diagram of the lowest electronic states of O_2 is shown in Chart 4. The sole nonvanishing SOC matrix element between the singlet and triplet states connects the $^1\Sigma_g^+$ excited state and the $M_S = 0$ level of the $^3\Sigma_g^-$ ground state.[40,45] Thus, the spin- and symmetry-forbidden $^1\Delta_g \rightarrow {}^3\Sigma_{g,M_S=0}^-$ transition (a) can borrow intensity from the spin-allowed $^1\Sigma_g^+ \rightarrow {}^1\Delta_g$ transition (b). In the free O_2 molecule, transition b is electric-quadrupole in nature and accordingly weak, but in solvents the radiative rate constant increases by several orders of magnitude because this transition becomes electric-dipole-allowed through collision of O_2 with solvent molecules.[45] By analogy, the asymmetric end-on binding mode of O_2 to Fe2 in complex **4** (Figure 3) should result in large

Chart 4. Schematic Energy Level Scheme for O_2

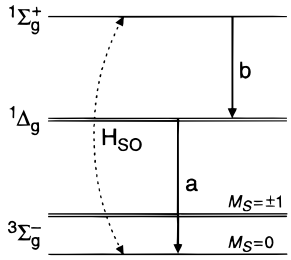

electronic factors for transition b and, consequently, transition a (Chart 4). Further, according to the energy-gap law for the limit of weak electron−phonon coupling[46] (which is the case for O_2) the nonradiative relaxation rate constant increases exponentially with decreasing reduced energy gap *p*, defined by the number of highest-energy vibrational quanta required to bridge the energy gap between the initial and final electronic states.[46] In complex **4** the relevant singlet and triplet states of O_2 are practically degenerate (*vide supra*). Thus, with the O−O stretch serving as the accepting mode, this leads to a small reduced energy gap *p* and, therefore, to a large rate constant for nonradiative $^1\Delta_g \rightsquigarrow {}^3\Sigma_g^-$ decay, probably much larger than in water where the $^1\Delta_g$ lifetime is only 3.3 μs.[45]

In summary, analysis of the spin state correlation for the conversion of oxyHr into deoxyHr leads to the following model. With progress along the reaction coordinate from oxyHr (**1**) to **4** (Figure 2), the total spin state of the system increases because of the more favorable electron correlation in the triplet vs singlet states of O_2 and the decrease in exchange coupling between the two Fe centers due, primarily, to protonation of the oxo bridge in the ETPT event (Figure 2, region II). While the stabilization of higher spin states favors release of triplet dioxygen from oxyHr (region III), the nature of the bonding interactions of singlet and triplet O_2 with deoxyHr (Chart 3) is such that one component of $^1\Delta_g$ dioxygen is sufficiently stabilized in energy to cause a partial initial production of singlet O_2; however, this species should decay extremely rapidly to the triplet ground state because of the high efficiency of nonradiative multiphonon relaxation processes for O_2 partly bonding to Fe2.

Energetics. Experimental studies of the interconversion of oxyHr and deoxyHr are extensive;[1,10] however, suitable data for an evaluation of our proposed model are very limited. For the protein from *P. gouldii*, an activation enthalpy of $\Delta H^\ddagger = 20.6$ kcal/mol was obtained for the first-order deoxygenation process of oxyHr.[37] This value agrees well with the calculated value of ~20 kcal/mol, estimated from the energy difference between **2** and oxyHr (**1**) under the assumption that the PT tunneling process does not contribute to $\Delta H^\ddagger$ (although, formally, structure **3** represents the transition state).[47] It should be noted, however, that the good correspondence with the experimental value is fortuitous. A quantitative analysis of the energy profile for the deoxygenation process of oxyHr would require the use of more complete active site models as well as a correction for zero-point vibrational energies. This is beyond

(44) McCarthy, P. J.; Güdel, H. U. *Coord. Chem. Rev.* **1988**, *88*, 69.
(45) Minaev, B. F.; Ågren, H. *J. Chem. Soc., Faraday Trans.* **1997**, *93*, 2231.
(46) Riesberg, L. A.; Moos, H. W. *Phys. Rev.* **1968**, *174*, 429.
(47) From Figure 2 (region III) the energy of each spin state considered increases from structure **4** to deoxyHr (**5**). Thus, under the assumption that the PT tunneling process does not contribute to $\Delta H^\ddagger$, oxygenation of deoxyHr should be activationless, yet an experimental value of $\Delta H^\ddagger = 8.2$ kcal/mol was obtained.[37] Presumably, this discrepancy is due primarily to (i) reoptimization of only a subset of atomic positions in the calculation of the reaction profile and (ii) the approximate nature of the models used (i.e., conformational changes of the protein in the oxygenation reaction of deoxyHr can make a substantial contribution to $\Delta H^\ddagger$).

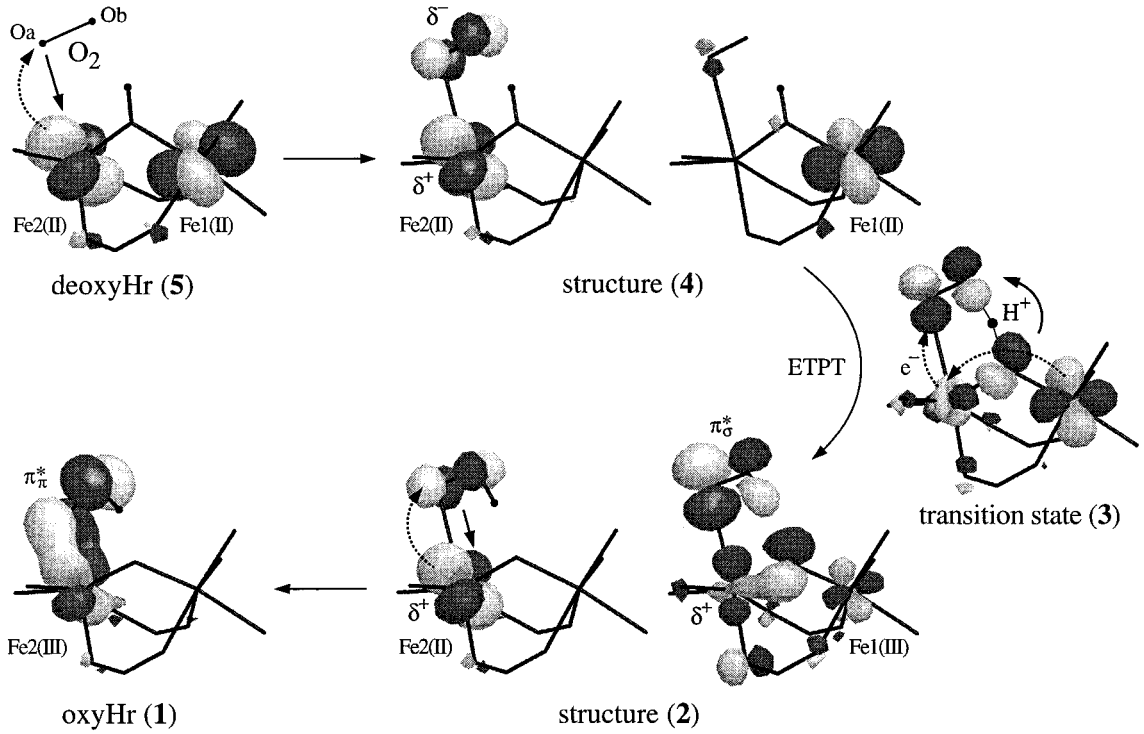

Figure 5. Schematic illustration of the relevant steps for O_2 binding to deoxyHr. Pathways for electron and proton transfers are indicated by curved dotted and solid arrows, respectively (ETPT: concerted proton-coupled electron transfer).

the scope of the present study where the focus is on electronic structure contributions to the reactivity of Hr with O_2. For this study reasonable bonding descriptions of the deoxyHr and oxyHr active sites, as obtained in the accompanying paper,[12] are of primary importance.

4. Discussion

Though the desire to obtain molecular-level insight into the fascinating process of reversible O_2 binding to hemerythrin (Hr) has driven a wide range of spectroscopic and crystallographic studies on the two physiologically relevant forms deoxyHr and oxyHr over the past few decades,[1,10] surprisingly little is known about this reaction. In the present study the reaction coordinate for O_2 release from oxyHr was explored through density functional calculations that correlate between the experimentally calibrated electronic structure descriptions of oxyHr and deoxyHr generated in the accompanying paper.[12]

Formally, O_2 release from oxyHr corresponds to a proton-coupled two-electron transfer process occurring at a single metal center (Chart 1). From Figure 3, the two electron transfer (ET) steps are coupled to distortions along two distinct coordinates. The first ET, a spin-down electron from the hydroperoxide to the coordinated iron (Fe2), occurs gradually with increasing Fe2−Oa distance (**1** → **2**). The ET pathway involves the hydroperoxide π^*_π orbital that is π-antibonding to the redox active orbital on Fe2 (Figure 3, top); thus, it involves the same set of orbitals that produce the dominant Fe2−hydroperoxide bonding interaction in oxyHr.[12] From oxyHr (**1**) through **2** (Figure 3) to deoxyHr[12] the orientation of the Fe2-based acceptor orbital is virtually unchanged, indicating that the ligand environment of Fe2 properly orients the redox active orbital on that center.

The second ET, a spin-up electron from the π^*_σ orbital of the hydroperoxide (that is formally already one-electron-oxidized) to the noncoordinated iron (Fe1), is coupled to the proton transfer (PT) from the O_2 moiety to the bridging oxide (Figure 3, structures **2** → **4**), corresponding to a concerted proton-coupled electron transfer (ETPT). The calculated rate constant for the PT event is large, $k_{PT} \approx 7 \times 10^{11}$ s^{-1}, consistent with the small observed kinetic isotope effects for O_2 binding and release of 1.0 and 1.2, respectively.[29] The corresponding O_2 → Fe1 ET occurs adiabatically,[38] i.e., gradually with distortion along the proton coordinate, and involves the Fe2−O−Fe1 mixed σ/π superexchange pathway (Figure 3, structure **3** (top)) that makes the dominant contribution to the antiferromagnetic exchange coupling in oxyHr.[12] Significantly, this ET pathway (i) affords a large electronic coupling matrix element between the π^*_σ orbital of O_2 binding to Fe2 and the redox active, *low-lying* Fe1-centered d_π orbital, and (ii) it is virtually eliminated upon protonation of the bridging oxide in deoxyHr. Therefore, in the process of dioxygen binding to deoxyHr, transfer of the extra electron from Fe1(II) to the O_2 species can only occur in concert with the PT. In linear dimers a similar mixed σ/π superexchange pathway is eliminated by symmetry, emphasizing the importance of a multiply bridged active site in Hr to produce the bent Fe−O−Fe unit ($\angle = 125°$).[4]

An interesting aspect of O_2 release from oxyHr concerns the correlation of spin states.[48] In oxyHr strong antiferromagnetic exchange coupling between the two Fe(III) centers gives rise to a large stabilization of the singlet ($S = 0$) ground state.[12] The first ET from the hydroperoxide to Fe2 greatly weakens this coupling by reducing Fe1 → Fe2 electron delocalization, leading to a substantial decrease in exchange splitting of the ground state from oxyHr (**1**) to complex **2** (Figure 2, region I). In the second, proton-coupled ET event **2** → **4** the O_2 species is formally reduced to dioxygen where the triplet vs singlet state is largely stabilized by exchange, and concomitantly, protonation of the bridging oxide results in a further decrease in exchange coupling between the two Fe centers. Because of the favorable bonding interaction of triplet O_2 with the ferromagnetically rather than the antiferromagnetically coupled diferrous site in

(48) Armentrout, P. B. *Science* **1991**, *251*, 175.

complex **4** (Chart 3), the total spin state of the system increases in steps of $\Delta S = 1$ along the reaction coordinate from **2** to **4** (note that changes in the spin state involve the irons where spin−orbit coupling effects are significant). As a result, oxyHr preferentially releases triplet O_2; however, despite the removal of one electron from each of the two peroxide π^* orbitals with progress along the reaction coordinate,[49−51] initially some singlet O_2 will also be produced due to the favorable bonding interaction of this species with the antiferromagnetically coupled diferrous site (Chart 3). Because of the asymmetric end-on binding mode of the O_2 moiety to a single Fe center at the active site of Hr (Figure 3, structure **4**), the efficiency of nonradiative multiphonon relaxation processes should be very high, however, resulting in a rapid decay to the triplet ground state of the limited amount of singlet dioxygen produced.

Figure 5 schematically summarizes our proposed mechanism for O_2 *binding* to deoxyHr (i.e., the reverse reaction of O_2 release from oxyHr discussed above). The dioxygen molecule approaches along the open coordination site of the five-coordinate Fe2 center of deoxyHr (**5**). With decreasing Fe2−Oa distance, a weak bonding interaction develops between the redox active orbital on Fe2 and the π^*_π orbital of O_2 (see the accompanying paper for a discussion of the electronic structure of deoxyHr[12]). As a consequence, the pK_a of the bridging hydroxide decreases, and eventually, a situation is found in which the proton can tunnel from the bridging hydroxide (structure **4**) to the O_2 species (structure **2**), the two proton positions being isoenergetic. In the course of this event, the redox active orbital of Fe1 rotates to maximize the π-bonding interaction with the bridging oxide (whose orbitals shift to higher energy upon deprotonation), and the extra electron of Fe1 gradually transfers to the π^*_σ orbital of the O_2 moiety through the Fe1−O−Fe2 mixed π/σ superexchange pathway (structure **3**). This process corresponds to a concerted proton-coupled electron transfer (ETPT) where the distortion along the proton coordinate drives the oxidation of Fe1(II) (structure **4**) to Fe1(III) (structure **2**). In the final step, a decrease in the Fe2−Oa distance to the equilibrium value of ∼2.0 Å formally drives the second ET, from Fe2 to the π^*_π orbital of O_2H, yielding the terminal hydroperoxide at the oxo-bridged diferric site of oxyHr (**1**). The thermodynamic driving force for O_2 binding to deoxyHr (Figure 2, **5** → **1**)) is high,[37] largely because of the formation of the very stable μ-oxo diiron(III) unit and the associated increase in antiferromagnetic coupling with progress along the reaction coordinate, which leads to a net stabilization of the singlet ground state for oxyHr.

Acknowledgment. Financial support by the NSF-Biophysics Program Grant MCB 9816051 is gratefully acknowledged.

Supporting Information Available: Energy level diagram from a BS calculation on μ-OH,O_2, overlay plot of the optimized μ-O, Ob, and H positions for fixed Fe2−Oa distances, plot of the calculated Mulliken charge of the proton for the interconversion of oxyHr and deoxyHr, and tables reporting the coordinates of all the models used for the calculations (PDF). This material is available free of charge via the Internet at http://pubs.acs.org.

JA992234S

(49) Note that the fact that singlet O_2 is also produced upon removal of one electron from each of the two peroxide π^* orbitals was not considered in previous computational studies of dioxygen release from multinuclear metal complexes.[50,51]

(50) Proserpio, D. M.; Hoffmann, R.; Dismukes, G. C. *J. Am. Chem. Soc.* **1992**, *114*, 4374.

(51) Nishida, Y. *Inorg. Chim. Acta* **1988**, *152*, 73.